Available online at www.sciencedirect.com
SCIENCE DIRECT®
Journal of Sound and Vibration 286 (2005) 729–743
JOURNAL OF SOUND AND VIBRATION
www.elsevier.com/locate/jsvi

Flexural wave scattering and dynamic stress concentration in a heterogeneous plate with multiple cylindrical patches by acoustical wave propagator technique ☆

S.Z. Peng*

School of Mechanical Engineering, Centre for Acoustics, Dynamics and Vibration, The University of Western Australia, 35 Stirling Highway, Crawley, WA 6009, Australia

Received 12 December 2003; received in revised form 18 June 2004; accepted 16 October 2004
Available online 5 January 2005

Abstract

This paper presents the acoustical wave propagator technique to describe the flexural wave propagation and scattering in an elastic plate with multiple cylindrical patches. The wave propagation patterns in the presence of these patches are used to investigate dynamic stress concentration. An improved combined scheme of Chebyshev polynomial expansion and fast Fourier transformation compared with the exact analytical solutions is found to be effective in predicting the distribution of dynamic stress concentration. The dynamic stress concentration factors around the patches in the time domain are also discussed in detail.

1. Introduction

Due to the effects of discontinuities on dynamic stress concentration, scattering problems around these obstacles have received quite a lot of attention. Kirsch [1] pioneered the study of the stress concentration around a circular hole in an infinite plate under a uniform longitudinal tension. Afterwards, Ying and Truell [2] studied the scattering of sound waves by a spherical scatterer in an elastic medium. Kato [3] and White [4] considered the effect of a cylindrical

☆ Presented in part at the Tenth International Congress on Sound and Vibration, 7–10 July 2003, Stockholm, Sweden.

*Tel.: +61 8 6488 1901; fax: +61 8 6488 1024.
E-mail address: speng@mech.uwa.edu.au (S.Z. Peng).

0022-460X/$ - see front matter
doi:10.1016/j.jsv.2004.10.015

obstacle on wave scattering. The analytical study of dynamic stress concentrations was carried out by Nishimura and Jimbo [5]. They determined the stress in the vicinity of a spherical inclusion in elastic solid, which was subjected to a dynamical tensile-compressive force with harmonic time variation. Pao and Chao [6,7] investigated the flexural wave diffractions by a cavity in an elastic plate based on Mindlin's theory. Meanwhile, Radkowski [8] discussed the stresses in a plate containing a ring of circular holes and a central circular hole. Durelli and Riley [9] studied experimentally the stress distribution on the boundary of a circular hole in a large plate using a low-modulus model material in a combined photoelasticity and grid analysis. Recently, Leviatan et al. [10] presented a source-model technique to investigate the scattering of time-harmonic flexural wave in a heterogeneous thin plate. However, these studies were only limited to a scatterer with simple shape. It is noted that Tadeu et al. [11–13] applied the boundary element method (BEM) to evaluate 3D scattering by multiple cylindrical cavities buried in an elastic medium. They considered complex BEM to determine the unspecified coefficients and found the solution of the wave equation. Due to its complex and limitation, hence, there is still a need for the development of effective and accurate methods to investigate problems including dynamic stress concentration and pre-fatigue at structural discontinuity and transient energy exchange across the coupling boundaries.

Most recently, Pan and Wang [14] developed the numerical scheme in quantum theory by Tal-Ezer and Kosloff [15] into a new expansion scheme named as the acoustical wave propagator (AWP). This scheme was found to be highly accurate and computationally effective in predicting the acoustical wave propagation. They described the propagation and scattering of one-dimensional acoustical wave packets. Furthermore, Peng and Pan extended this technique to investigate the time-domain flexural wave propagation in thin plate [16], a stepped plate [17], and dynamic stress concentration on a ribbed plate [18] and patched plate [19] considered boundary conditions. However, there is a limit due to the dynamic range of expansion functions in this method. An improved expansion scheme was described in Ref. [20]. The main objective of the present paper is to investigate the time-domain wave propagation and scattering, and dynamic stress concentration in a heterogeneous thin plate with multiple cylindrical patches by the AWP technique with this improved expansion scheme.

2. Theory of the AWP technique

Plates with bolts or rivets are regarded as common components of many practical engineering structures. In this paper, these plates are modelled by a plate with N cylindrical patches, which are arranged linearly (see Fig. 1). Area A_i is introduced to describe the region of the ith patch, where $i = 1, 2, \ldots, N$. The patches are made of the same material as the plate. Although the radius of the patches is comparable with the plate thickness, these patches may affect not only the transverse shear deformation in their vicinity, but also in the whole plate. In this paper, investigation on the wave propagation and dynamic stress concentration is based on the classical Kirchhoff's theory. When disturbed, wave motion occurs in the plate. The wave motion generates dynamic moments and shear forces which result in internal stresses.

The plate is subjected to a distributed external pressure load $P(x_{\text{in}}, y_{\text{in}}, t)$ as a function of time. Two kinds of moments, namely bending moments M_x and M_y, and twisting moments M_{xy} and

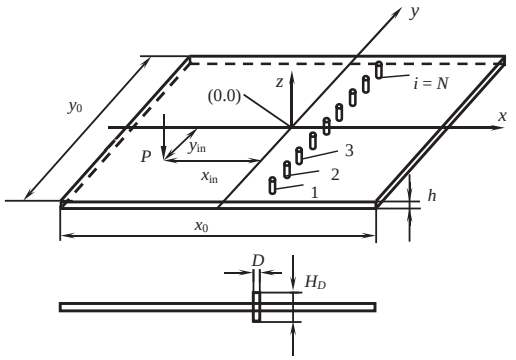

Fig. 1. Schematic of a thin plate with multiple cylindrical patches.

M_{xy}, are involved. The maximum strains in a plate occur at its surfaces. Therefore, for any given position and instant, the strain components are given by Morse and Ingard [21]

$$\varepsilon_x = \pm\frac{h(x,y)}{2}\frac{\partial^2 W}{\partial x^2},$$
$$\varepsilon_y = \pm\frac{h(x,y)}{2}\frac{\partial^2 W}{\partial y^2},$$
$$\varepsilon_{xy} = \pm h(x,y)\frac{\partial^2 W}{\partial x \partial y}, \tag{1}$$

where

$$h = h(x,y) = \begin{cases} h_D & (x,y) \subseteq A_i|_{i=1\sim N} \\ h & \text{otherwise} \end{cases},$$

where h_D and h denote the thicknesses of the patches and the plate, respectively. The principal stress at a given point on the plate surface occurs on the so-called principal planes. In general, these are not parallel to the coordinate planes. The principal stress σ_P can be calculated by

$$\sigma_P = \frac{E}{2}\left(\frac{\varepsilon_x + \varepsilon_y}{1-\upsilon} + \frac{\sqrt{(\varepsilon_x - \varepsilon_y)^2 + (\varepsilon_{xy})^2}}{1+\upsilon}\right), \tag{2}$$

where E and υ denote the Young's modulus and Poisson's ratio of the plate, respectively.

The derivatives of the moments are

$$\frac{\partial M_x}{\partial t} = -D\left[\frac{\partial^2 V}{\partial x^2} + \upsilon\frac{\partial^2 V}{\partial y^2}\right],$$
$$\frac{\partial M_y}{\partial t} = -D\left[\frac{\partial^2 V}{\partial y^2} + \upsilon\frac{\partial^2 V}{\partial x^2}\right],$$
$$\frac{\partial M_{xy}}{\partial t} = -D(1-\upsilon)\left[\frac{\partial^2 V}{\partial x \partial y}\right], \tag{3}$$

where $D = (Eh^3(x,y)/12(1-\upsilon^2))$ is the flexural rigidity of the plate. $V = \partial W/\partial t$ is the velocity of the plate in the z-axis.

The governing equation for the motion of this structure is given by

$$\rho h \frac{\partial V}{\partial t} = \frac{\partial^2 M_x}{\partial x^2} + 2\frac{\partial^2 M_{xy}}{\partial x \partial y} + \frac{\partial^2 M_y}{\partial y^2} + P(x,y,t), \tag{4}$$

where ρ is the mass per unit area of the plate. In this paper, only dynamic time-dependent response to initial conditions is considered. Therefore, $P(x,y,t) = 0$.

To derive the acoustical wave propagator for flexural waves in a thin plate, a state vector ϕ which consists of angular velocities, the bending moments (i.e. $M_x(x,y,t)$, $M_y(x,y,t)$) and one of the twisting moments, $M_{xy}(x,y,t)$, of the plate is selected. The system state equation can be obtained by combining Eqs. (3) and (4)

$$\frac{\partial}{\partial t}\begin{bmatrix} V & M_x & M_y & M_{xy} \end{bmatrix}^{\mathrm{T}} = -\hat{H}\begin{bmatrix} V & M_x & M_y & M_{xy} \end{bmatrix}^{\mathrm{T}}, \tag{5}$$

where

$$\hat{\mathbf{H}} = \begin{bmatrix} 0 & -\frac{1}{\rho h(x,y)}\frac{\partial^2}{\partial x^2} & -\frac{1}{\rho h(x,y)}\frac{\partial^2}{\partial y^2} & -\frac{2}{\rho h(x,y)}\frac{\partial^2}{\partial x \partial y} \\ D\left(\frac{\partial^2}{\partial x^2} + \upsilon\frac{\partial^2}{\partial y^2}\right) & 0 & 0 & 0 \\ D\left(\frac{\partial^2}{\partial y^2} + \upsilon\frac{\partial^2}{\partial x^2}\right) & 0 & 0 & 0 \\ D(1-\upsilon)\frac{\partial^2}{\partial x \partial y} & 0 & 0 & 0 \end{bmatrix}. \tag{6}$$

Thus, Eq. (5) can be rewritten by integrating with respect to time

$$\phi(x,y,t) = \mathrm{e}^{-(t-t_0)\hat{\mathbf{H}}}\phi(x,y,t_0), \tag{7}$$

where $\mathrm{e}^{-(t-t_0)\hat{\mathbf{H}}}$ is defined as the acoustical wave propagator (AWP) for flexural waves in thin plates. The state vector $\phi(x,y,t)$ of acoustical wave at any time t can be evaluated by the operation of the AWP subjected to the initial state vector $\phi(x,y,t_0)$. Since the material properties are defined as a function of position, it is worth noting that the effect of boundaries and spatial variation of the acoustical media are readily included in the system operator $\hat{\mathbf{H}}$. This advantage is particularly useful to some structures including the complex continuity conditions and boundary conditions.

3. Comparison between the AWP technique and exact analytical solution

3.1. The improved combined scheme of Chebyshev polynomial expansion and fast Fourier transformation

A detailed description of the acoustical wave propagator with the modified Chebyshev polynomials was given by Peng and Pan [16–18]. In this paper, an improved expansion scheme to implement the operation of the exponential propagator is introduced. Eq. (7) can be

approximated by a sum of $N+1$ polynomials such that

$$\phi(x,y,t) = \mathrm{e}^{-(t-t_0)\hat{\mathbf{H}}}\phi(x,y,t_0) \approx \sum_{n=0}^{N} j^n c_n J_n(R) T_n(j\hat{\mathbf{H}}')\phi(x,y,t_0), \tag{8}$$

where $R=(t-t_0)\lambda_{\max}$ and $\hat{\mathbf{H}}' = \hat{\mathbf{H}}/\boldsymbol{\lambda}_{\max}$, $\boldsymbol{\lambda}_{\max}$ is the maximum eigenvalue of the system operator and $c_n = 2$ except for $c_0 = 1$. $J_n(R)$ is the Bessel function. $T_n(j\hat{\mathbf{H}}')$ represents the nth degree Chebyshev polynomial calculated by

$$\begin{aligned} &T_0(j\hat{\mathbf{H}}') = I; \quad T_1(j\hat{\mathbf{H}}') = j\hat{\mathbf{H}}', \\ &T_{n+1}(j\hat{\mathbf{H}}') = 2j\hat{\mathbf{H}}' T_n(j\hat{\mathbf{H}}') - T_{n-1}(j\hat{\mathbf{H}}'), \text{ when } n>1. \end{aligned} \tag{9}$$

A new set of polynomial was introduced to implement the calculation from complex numbers to real value:

$$\widehat{T}_n(\hat{\mathbf{H}}') = j^n T_n(j\hat{\mathbf{H}}'), \tag{10}$$

where $\widehat{T}_n(\hat{\mathbf{H}}')$ can be calculated by

$$\begin{aligned} &\widehat{T}_0(\hat{\mathbf{H}}') = I; \quad \widehat{T}_1(\hat{\mathbf{H}}') = -\hat{\mathbf{H}}', \\ &\widehat{T}_{n+1}(j\hat{\mathbf{H}}') = -2\hat{\mathbf{H}}'\widehat{T}_n(\hat{\mathbf{H}}') + \widehat{T}_{n-1}(\hat{\mathbf{H}}'), \text{when } n>1. \end{aligned} \tag{11}$$

Therefore, Eq. (8) can be rewritten as

$$\phi(x,y,t) = \sum_{n=0}^{N} c_n J_n(R)\widehat{T}_n(\hat{\mathbf{H}}')\phi(x,y,t_0). \tag{12}$$

Thus, the AWP operation becomes the calculation of the normalized system operator $\hat{\mathbf{H}}'$, which mainly involves the evaluation of spatial derivatives. Therefore, the spatial derivatives of function $\phi(x,y,t)$ can be calculated by the Fourier transformation.

In addition, the following Fourier and inverse Fourier transformations are used to calculate the spatial derivatives of function $\phi(x,y,t)$:

$$\begin{aligned} &\frac{\partial^2}{\partial x^2}\phi(x,y,t) = F^{-1}\{(jk_x)^2 F[\phi(x,y,t)]\}, \\ &\frac{\partial^2}{\partial y^2}\phi(x,y,t) = F^{-1}\{(jk_x)^2 F[\phi(x,y,t)]\}, \\ &\frac{\partial^2}{\partial x\partial y}\phi(x,y,t) = F^{-1}\{(jk_x)(jk_y) F[\phi(x,y,t)]\}, \end{aligned} \tag{13}$$

where $F[\,]$ and $F^{-1}\{\,\}$ represent the Fourier transformation and inverse Fourier transformation, respectively. k_x and k_y are the bending wave numbers in the x- and y-axis, respectively.

The accuracy of the Fourier transformation method for evaluating spatial derivatives had been examined in Refs. [16,17]. When the spatial sampling intervals Δx and Δy are given, the discrete

Fourier expansion of a wave packet supports the maximum wave number (equivalent to the shortest wavelength or the highest frequency).

3.2. The exact analytical solution

From Eq. (3) and Eq. (6), the complete information of the whole system at any time and any point can be obtained. In particular, the principal stress of the plate can be calculated. The numerical convergence and stability of old scheme have been examined in Refs. [16,17]. To describe the benefit of this improved scheme, the predicted result of the principal stress is compared with the exact analytical solution in a thin plate without patches. The displacement with an analytical solution is given by Antonio and Tadeu [22]

$$W(r,t)=\frac{f_0}{1+\tau^2}\mathrm{e}^{(-\mu^2/(1+\tau^2))}\left\{\cos\left(\frac{\mu^2\tau}{1+\tau^2}\right)+\tau\,\sin\left(\frac{\mu^2\tau}{1+\tau^2}\right)\right\}, \tag{14}$$

where $\tau=bt/\sigma^2, \mu=r/2\sigma$. $W(r,t)$, σ and f_0 denote the deflection displacement of the plate in the z-axis, Gaussian factor and a constant, respectively.

From Eq. (14), the first- and second-order derivatives of $W(r,t)$ can be obtained:

$$\begin{aligned}\frac{\partial W(r,t)}{\partial r}&=\frac{f_0\mu}{\sigma(1+\tau^2)^2}\mathrm{e}^{(-(\mu^2/1+\tau^2))}\\&\quad\times\left\{(\tau^2-1)\cos\left(\frac{\mu^2\tau}{1+\tau^2}\right)-2\tau\,\sin\left(\frac{\mu^2\tau}{1+\tau^2}\right)\right\},\\\frac{\partial^2 W(r,t)}{\partial r^2}&=\frac{f_0}{\sigma^2(1+\tau^2)^3}\mathrm{e}^{(-(\mu^2/1+\tau^2))}\\&\quad\times\begin{bmatrix}\left(\frac{\tau^4-6\mu^2\tau^2+2\mu^2-1}{2}\right)\cos\left(\frac{\mu^2\tau}{1+\tau^2}\right)\\+\tau(3\mu^2-\mu^2\tau^2-1-\tau^2)\sin\left(\frac{\mu^2\tau}{1+\tau^2}\right)\end{bmatrix}.\end{aligned} \tag{15}$$

Then, the stresses can be calculated by

$$\begin{aligned}\sigma_r&=-\frac{Eh}{2(1-\upsilon^2)}\left\{\frac{\partial^2 W}{\partial r^2}+\upsilon\frac{1}{r}\frac{\partial W}{\partial r}\right\},\\\sigma_\theta&=-\frac{Eh}{2(1-\upsilon^2)}\left\{\frac{1}{r}\frac{\partial W}{\partial r}+\upsilon\frac{\partial^2 W}{\partial r^2}\right\},\tau_{r\theta}=0.\end{aligned} \tag{16}$$

In treating principal stresses it is often useful to order them. In this paper, the normal stress having the largest algebraic value at a given point is only considered. The principal stress is calculated by

$$\sigma_P=\frac{\sigma_r+\sigma_\theta+\sqrt{(\sigma_r-\sigma_\theta)^2+4\tau_{r\theta}}}{2}, \tag{17}$$

when $\sigma_r>\sigma_\theta$, $\sigma_{\mathrm{P}}=\sigma_r$, whereas $\sigma_P=\sigma_\theta$. When $t=0.034\,\mathrm{s}$, the propagation of the wave packet covers the observation area ($-5\,\mathrm{m}\leqslant x\leqslant 5\,\mathrm{m}$ and $-5\,\mathrm{m}\leqslant y\leqslant 5\,\mathrm{m}$). Fig. 2 shows the absolute error

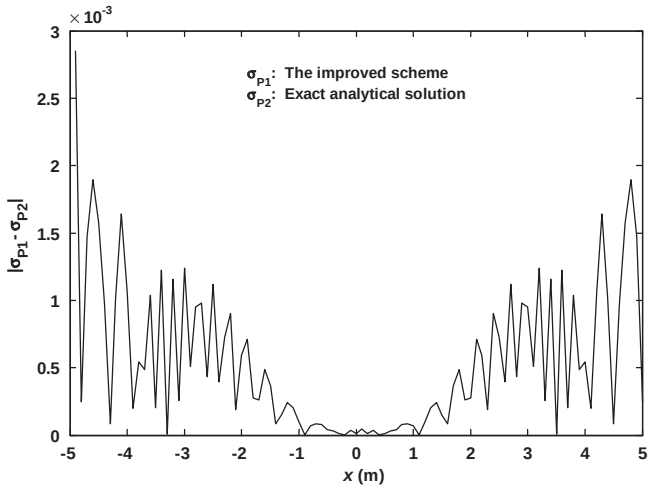

Fig. 2. Comparison between the improved scheme and exact analytical solution when $y = 0\,\mathrm{m}$ and $t = 0.034\,\mathrm{s}$.

of the principal stress between the numerical solution obtained by this improved scheme and the exact analytical solution. This new scheme is found to be highly accurate and computationally effective. Therefore, this improved scheme offers an opportunity for the study of dynamic stress concentration and time-domain energy flow in large complex structures. The aim of this paper is to focus on investigating dynamic stress concentration in a two-dimensional thin plate with multiple patches.

4. Numerical results

In the following numerical simulations, a steel plate is considered. Its properties are as follows: $E = 216\,\mathrm{GPa}$, $v = 0.3$, $h = 0.002\,\mathrm{m}$, $N = 9$, $h_D = 0.005\,\mathrm{m}$ and $\rho = 7800\,\mathrm{kg/m^3}$. Cylindrical patches with 1 m separations are located at $x = 1\,\mathrm{m}$ along the y-axis. The radius of the patches is 0.1 m, and the initial displacement point is at $(x_{\mathrm{in}},y_{\mathrm{in}}) = (0,0)\,\mathrm{m}$.

To demonstrate the implementation of AWP for an initial wave packet in the plate, the following initial state vector is used:

$$\phi(x,y,0) = \left[0 \quad M_x(x,y,t) \quad M_y(x,y,t) \quad M_{xy}(x,y,t)\right]^{\mathrm{T}}, \tag{18}$$

where $M_x(x,y,0)$, $M_y(x,y,0)$ and $M_{xy}(x,y,0)$ are related to the initial displacement $W(x,y,0) = W_0 \mathrm{e}^{-((x^2+y^2)/4\sigma^2)}$. In the simulations, $W_0 = 0.001\,\mathrm{m}$, $\sigma = 0.1$, the grid size is 100, and the spatial sampling intervals $\Delta x = \Delta y$ are 0.1 m. A plate with infinite size in the x and y dimensions is used and the spatial ranges used to observe the evolution of wave packet are $-5\,\mathrm{m} \leqslant x \leqslant 5\,\mathrm{m}$ and $-5\,\mathrm{m} \leqslant y \leqslant 5\,\mathrm{m}$. It is noted that further increase the grid size will improve slightly the accuracy of the predicted results. To decrease the effect of numerical error on the predicted results, the discontinuity should be smoothed by the convolution with a Gaussian Function. Meanwhile, it is

very critical to choose reasonably the simulation values among the grid size, time step and the Gaussian factor in the convolution. The work in this direction is in progress.

Fatigue failures often occur in regions with high stress concentration, so an understanding of the distribution of the stress concentration is very useful in structural design. Fig. 3 shows the distribution of the principal stress σ_P (Eq. (2)) in the plate at various times. For a Gaussian wave packet used the principal stress at $t = 0$ s is concentrated at the center of the plate. As time increases, this stress concentration begins to spread out with decreased magnitude. When the first incident wave arrives the 5th patch, the scattered waves are produced and they superimpose with successive incident waves. It is observed that one sharp peak exists in the second ring wave. At $t = 0.02$ s, the incident waves arrive more patches and thus, more scattered waves are generated. Therefore, peaks exist around more patches. It is noted that, at $t = 0.034$ s, four areas with much larger magnitudes of stresses are showed clearly in Figs. 3(c) and (d). These distributions depend on the ratio of patch thickness to the plate thickness, the material properties of the plate, the radius of the patch, and the distance between the excitation point and the discontinuities.

To explain the patterns in Fig. 3, the total wave fields are analyzed and decomposed into two parts namely, the incident waves without the patches, and the scattered waves by the patches. They are defined as $\phi(x, y, t)^t = \phi(x, y, t)^i + \phi(x, y, t)^s$, where $\phi(x, y, t)$ represents the state vector of the plate. Superscripts i, s and t denote the incident, the scattered, and the total waves, respectively. The magnitude of combined wave field depends on the magnitudes of the incident

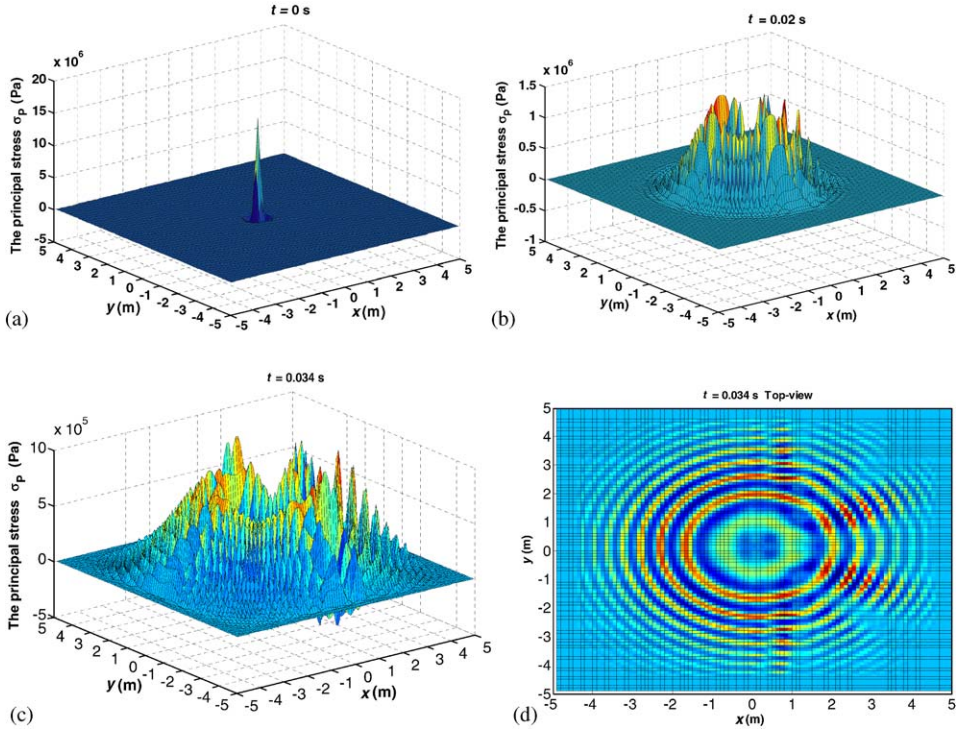

Fig. 3. Distribution of the principal stresses at different instants.

and scattered waves. The stress concentration peaks are due to the superposition of incident and scattered waves from the patches. The stress distributions without the patches are not given in this paper. Stress distributions of scattered waves are illustrated in Fig. 4. When $t = 0.01$ s, the incident waves reach the central patches, the scattered waves distribute near the behind of these patches. When time increases, more and more patches involve and cause a wider distribution. Fig. 4 explains reasonably the principal stress distribution of distributed flexural wave as shown in Fig. 3. The most interesting feature in Figs. 4(a) and (b) is that the spatial wave interference

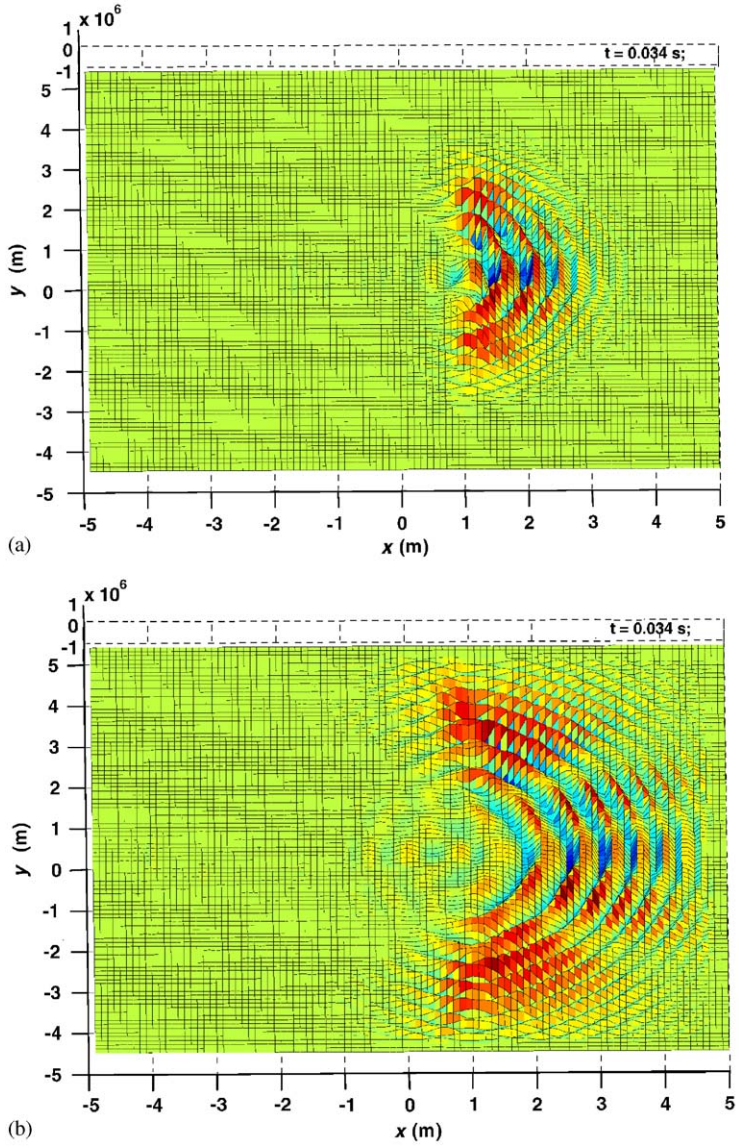

Fig. 4. Distribution of the scattered waves in plate at different instants.

pattern is much different from those obtained in a stepped plate [17]. The reason is that more waves pass through the gaps between the patches.

Stress concentration often occurs in regions near discontinuities. Due to the symmetry of this structure, half of these patches are chosen to observe the principal stresses as a function of time. Fig. 5 shows the distribution of the predicted points. Fig. 6 shows dynamic stresses of these predicted points. One observation is that, due to the distance difference between the predicted points and the initial wave packet, the maximum stress happens first in patch 5 in Fig. 6(e), then patch 4 in Fig. 6(d), patch 3 in Fig. 6(c), patch 2 in Fig. 6(b) and finally in patch 1 in Fig. 6(a). In each patch, the arriving time of the maximum dynamic in four predicted points I, II, III and IV depends on the distance between their locations and the initial wave packet. For example, for patch 5, the time sequence is Points 5_{I}, 5_{II} and 5_{IV}. Another observation is that the magnitudes of the maximum stress depend on the distance between the predicted points and the initial wave packet. Generally, the magnitudes decrease nonlinearly from patch 5 to patch 1. Due to the scattered wave from these patches, the dynamic stresses around these patches will change significantly. It is the reason that stress distribution should be considered not only the distance between the predicted points and the initial wave packet, but also the scattered effects. Furthermore, Figs. 6(f)–(h) show the effects of these patches on dynamic stresses.

The dynamic stress concentration factor is defined as the ratio of stress due to the total wave (with the patches) at a point to the stress due to the incident wave (without the patches) at the same point. Fig. 7 shows the dynamic stress concentration factors of 19 predicted points. For

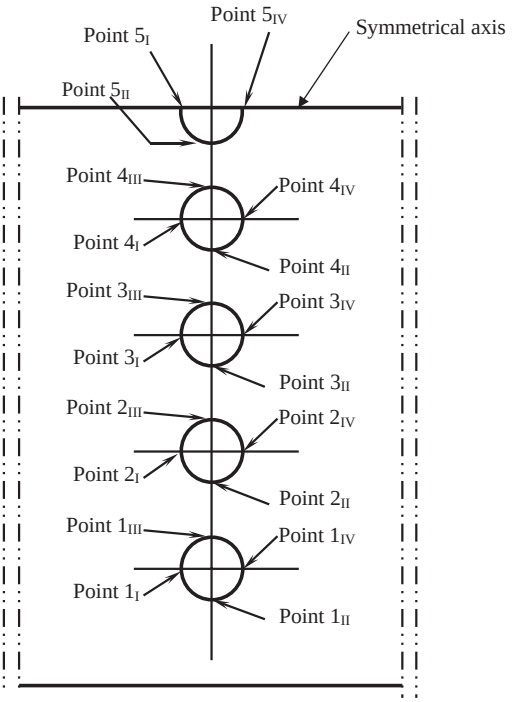

Fig. 5. Schematic of the predicted points.

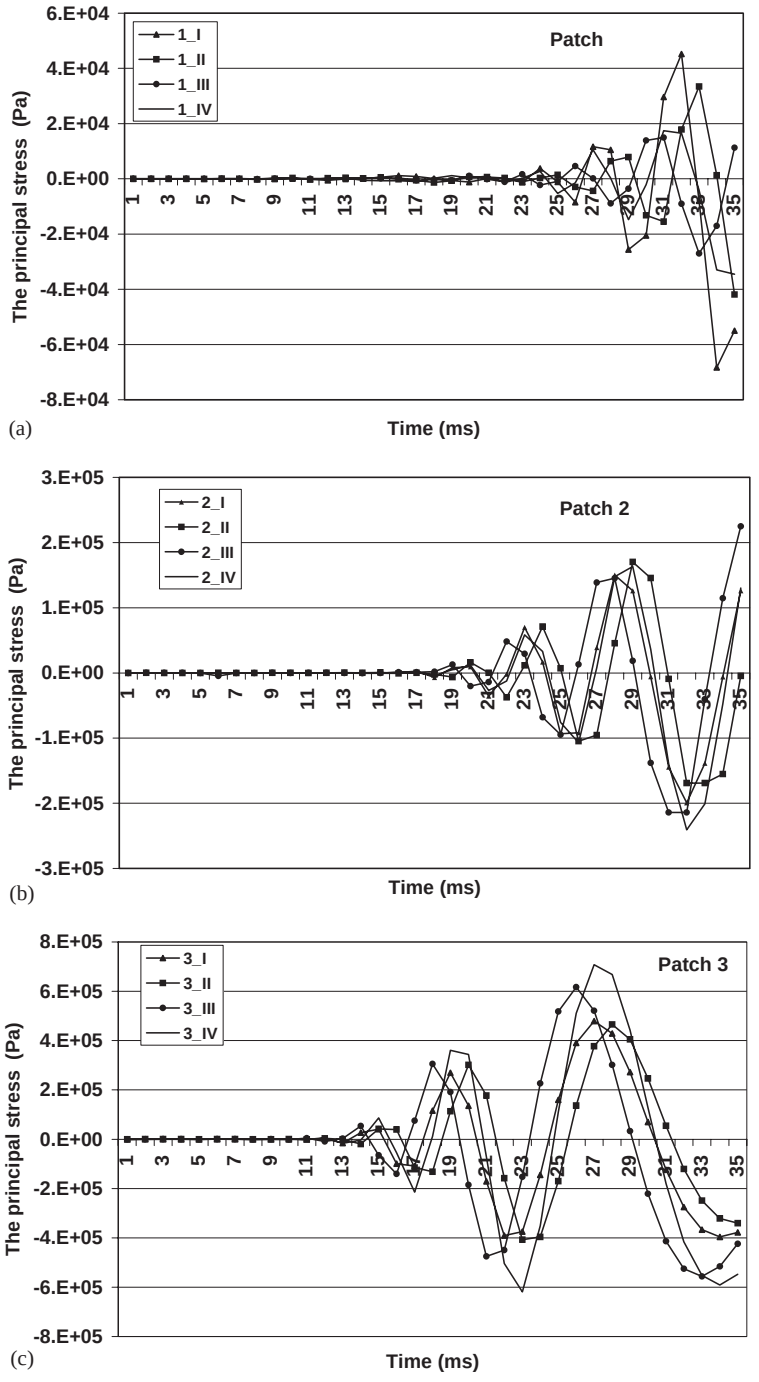

Fig. 6. Dynamic stresses of the predicted points.

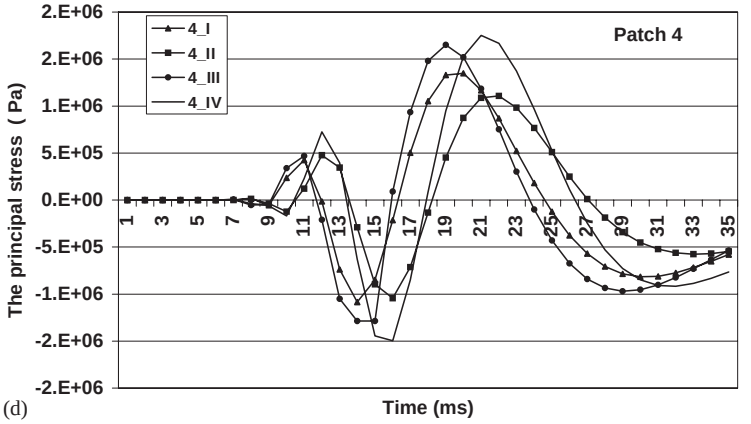

(d)

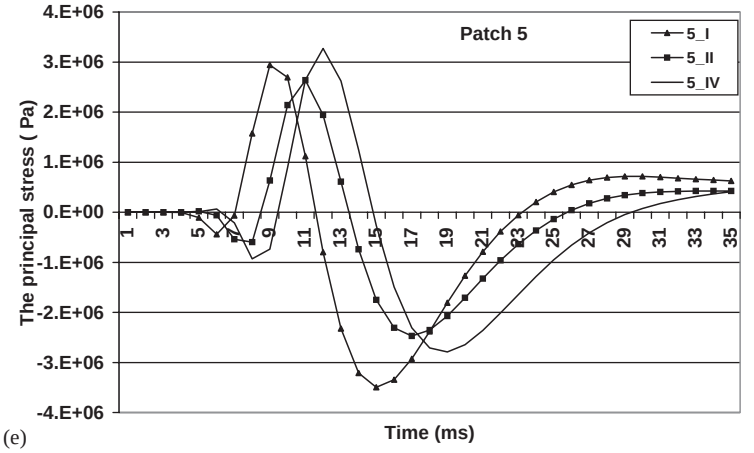

(e)

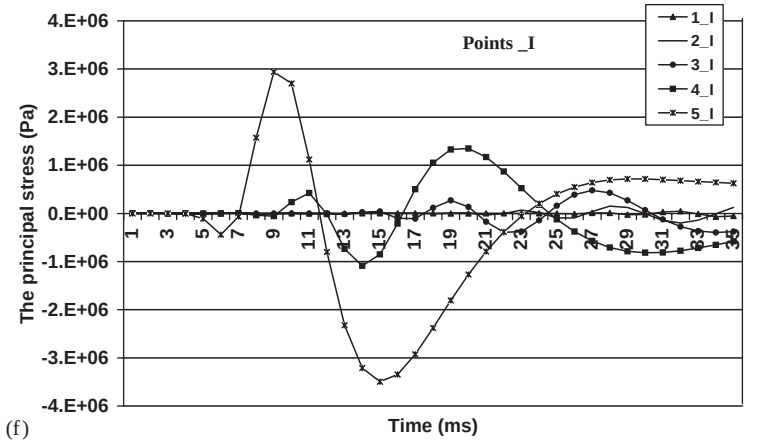

(f)

Fig. 6. (*Continued*)

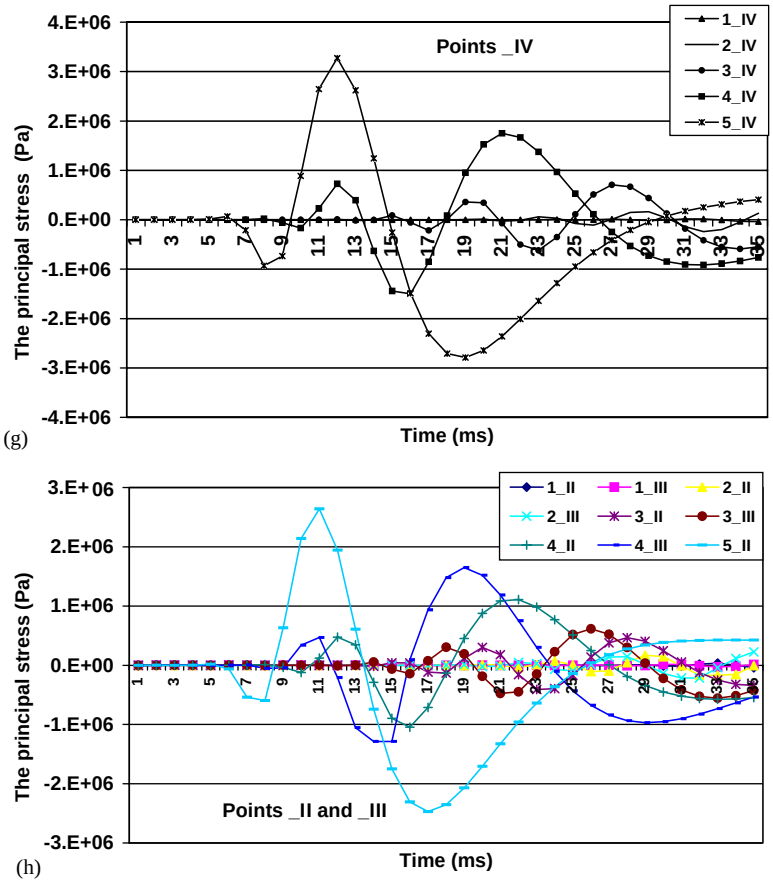

Fig. 6. (*Continued*)

most of these points, the dynamic stress concentration factors are larger than 1. It shows that the presence of these patches has great effects on stress distribution. At some points, the factor is as high as 2.5 (see Fig. 7). It is noted that the peak stresses between the cases with and without the patches are not occurring at the same instant. This is due to the interference of the incident wave and scattered waves. This technique supplies a method in the time-domain to find the point with the maximum dynamic stress concentration factor.

5. Conclusions

The acoustical wave propagator (AWP) technique is extended to describe the flexural wave scattering and dynamic stress concentration in a two-dimensional thin plate with multiple patches. Wave propagation patterns are presented to illustrate the maximum stress concentration in the presence of the patches, which simulate bolts or rivets. The main advantage of the AWP technique is no necessary to consider complex boundaries in numerical analysis. In particular, when the

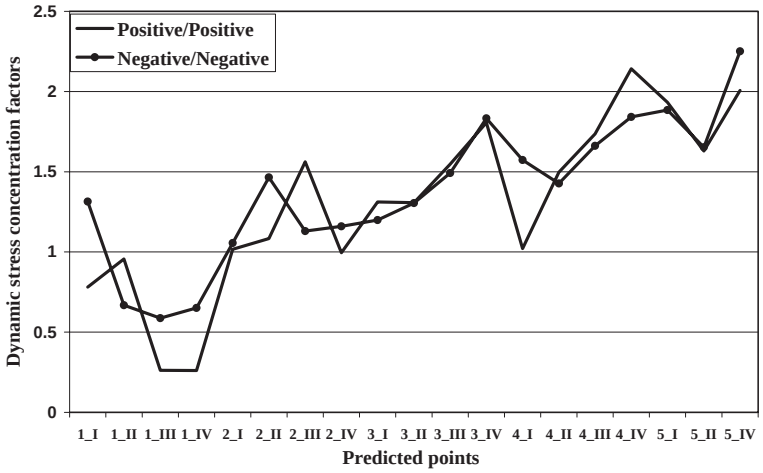

Fig. 7. Dynamic stress concentration factors of the predicted points.

exact analytical solution cannot be obtained, the improved combined scheme of Chebyshev polynomial expansion and fast Fourier transformation is more direct and elegant. Therefore, it provides a quick means for predicting the distribution of dynamic stress concentration in complex structures. Furthermore, this technique can be successfully used in the study of coupling loss factors and energy flow in coupling structures. The relevant work is under way.

Acknowledgments

The author is grateful to Professor J. Pan and Dr. K.S. Sum for valuable discussion and their help in numerical analysis. The author thanks the University of Western Australia for the financial support from the BANKWEST Postgraduate Research Award and DR JULIAN HUNKA Scholarship and Australian Postgraduate Research Scholarship.

References

[1] G. Kirsch, Die theorie der elastizität und die Bedürfnisse der Festigkeitskehre, *Zeitschirft des Vereines Deutscher Ingenieure* 42 (1898) 797.
[2] C.F. Ying, R. Truell, Scattering of a plane longitudinal wave by a spherical obstacle in an isotropically elastic solid, *Journal of Applied Physics* 27 (1956) 1086.
[3] K. Kato, Reflection of sound wave due to a hollow cylinder in an elastic body, *Memoirs of the Institute of Scientific and Industrial Research, Osaka University, Japan* 9 (1952) 16.
[4] R.M. White, Elastic wave scattering at a cylindrical discontinuity in a solid, *The Journal of the Acoustical Society of America* 30 (1958) 771.
[5] G. Nishimura, Y. Jimbo, A dynamical problem of stress concentration, *Journal of Faculty of Engineering, University of Tokyo, Japan* 24 (1955) 101.

[6] Y.H. Pao, C.C. Chao, Diffractions of flexural waves by a cavity in an elastic plate, *AIAA Journal* 2 (1964) 2004–2010.
[7] Y.H. Pao, Dynamic stress concentration in an elastic plate, *Journal of Applied Mechanics* 29 (1962) 299–305.
[8] P.P. Radkowski, Stresses in a plate containing a ring of circular holes and a central circular hole, *Journal of Applied Mechanics* 31 (1964) 277–282.
[9] A.J. Durelli, W.F. Riley, Stress distribution on the boundary of a circular hole in a large plate during passage of a stress pulse of long duration, *Journal of Applied Mechanics* 30 (1961) 245–251.
[10] Y. Leviatan, E.T. Erez, M.J. Beran, A source-model technique for analysis of flexural wave scattering in a heterogeneous thin plate, *The Quarterly Journal of Mechanics and Applied Mathematics* 45 (1992) 499–514.
[11] A.J.B. Tadeu, L. Godinho, P.F.A. Santos, Performance of the BEM solution in 3D acoustical wave scattering, *Advances in Engineering Software* 32 (2001) 629–639.
[12] J. Antonio, A.J.B. Tadeu, 3D scattering by multiple cylindrical cavities buried in an elastic formation, *European Journal of Mechanics A/Solids* 20 (2001) 367–383.
[13] A.J.B. Tadeu, P.F.A. Santos, *Scattering of Waves by Buried Cavities via Boundary Element Method*, EUROBEM, Wessex Institute of Technology, Southampton, UK, 1998 pp. 180–200.
[14] J. Pan, J.B. Wang, Acoustical wave propagator, *Journal of the Acoustical Society of America* 108 (2002) 481–487.
[15] Tal-Ezer, R. Kosloff, An accurate and efficient scheme for propagating the time-dependent Schrödinger equation, *Journal of Chemical Physics* 81 (1984) 3967–3971.
[16] S.Z. Peng, J. Pan, Acoustical wave propagator for time-domain flexural waves in thin plates, *Journal of the Acoustical Society of America* 115 (2004) 467–474.
[17] S.Z. Peng, J. Pan, A study of time-domain stress concentration in a plate with sharp change of section using the acoustical wave propagator technique, *Journal of the Acoustical Society of America*, 2004, in press.
[18] S.Z. Peng, Dynamic stress concentration in a ribbed plate using the acoustical wave propagator technique, *Journal of Sound and Vibration* 279 (2005) 75–88.
[19] S.Z. Peng, J. Pan, K.S. Sum, Acoustical wave propagator for time-domain analysis of flexural wave scattering and dynamic stress concentration in a heterogeneous plate with multiple cylindrical patches, *Proceedings of the Tenth International Congress on Sound and Vibration*, Stockholm, Sweden, July 7–10 2003, pp. 5021–5028.
[20] J. Pan, J.B. Wang, Further development of the acoustical wave propagator, *Proceedings of the Tenth International Congress on Sound and Vibration*, Stockholm, Sweden, July 7–10, 2003, pp. 5045–5053.
[21] M. Morse, K.U. Ingard, *Theoretical Acoustics*, McGraw-Hill, New York, 1968.
[22] K.F. Graff, *Wave Motion in Elastic Solids*, Clarendon press, Oxford, 1975.